Proceedings of the International Symposium on Physics of Materials (ISPMA 14), September 10–15, 2017, Prague

Structural Evolution of P92-Type Martensitic Steel during Creep at 650 °C

A. Fedoseeva*, I. Nikitin, N. Dudova and R. Kaibyshev
Belgorod National Research University, Pobeda 85, 308015 Belgorod, Russia

Microstructure and a dispersion of secondary phase particles were examined in P92-type steel after creep test at temperature of 650 °C and an applied stress of 80 MPa in grip, gauge and necked portions of specimens. Normalization at 1050 °C and tempering at 780 °C for 3 h led to the formation mixed structure consisting of tempered martensite lath structure and subgrains. Long-term aging for 9273 h led to the formation of fully subgrain structure but the average subgrain sizes after tempering and after long-term aging were nearly the same. The structural changes in the gauge and necked sections were characterized by transformation of the tempered martensite lath structure into relatively coarse subgrain one accompanied by the coarsening of $M_{23}C_6$ carbides and precipitation of the Laves phase. No significant effect of creep strain on particle coarsening was found.

DOI: 10.12693/APhysPolA.134.644

PACS/topics: 9%Cr martensitic steel, creep, aging, subgrains, polygonization

1. Introduction

Grade P92 (9Cr–2W–VNbB-type) steel is widely used as material for boilers and tubes of fossil power plants with service temperature of 600 °C [1, 2]. The high creep resistance of these high-chromium steels is associated with the formation of a tempered martensite lath structure (TMLS) during tempering at 720–780 °C. TMLS consists of prior austenite grains (PAG), packets, blocks, laths and contains a high density of dislocations and a dispersion of secondary phase particles. $M_{23}C_6$-type carbides and MX carbonitrides precipitate along boundaries and within ferritic matrix, respectively, during tempering, and the Laves phase particles, $Fe_2(W,Mo)$, precipitate at boundaries under creep conditions [1–7]. An increase in tempering temperature leads to an increase in the width of martensitic laths and coarsening of $M_{23}C_6$ particles and MX carbonitrides, which can be more stable during long-term aging and creep [8]. Thermal recovery upon long-term aging and creep could be accompanied by the transformation of nanoscale MX carbonitrides into the coarse Z-phase particles and coarsening of boundary $M_{23}C_6$ carbides and Laves phase [8, 9]. The coarsening of the boundary particles initiates the transformation of lath boundaries into subboundaries; the internal long-range strain fields originated from lath boundaries relive [8, 9]. The aim of the present work is to report structural characteristics of P92-type steel tempered at 780 °C after long-term aging and creep at 650 °C.

2. Material and methods

P92-type steel with the chemical composition (in wt%) of Fe_{bal}–0.1C–0.17Si–0.54Mn–8.75Cr–0.51Mo–1.6W–0.23V–0.07Nb–0.04N–0.003B was normalized at 1050 °C for 0.5 h followed by tempering at 780 °C for 3 h. Cylindrical specimen with a gauge length of 100 mm and a 10 mm diameter was crept until rupture at 650 °C and an applied stress of 80 MPa using an ATS2330 lever arm machine. Microstructural characterization was performed in the grip, gauge and necked portions of ruptured specimen using a JEM-2100 transmission electron microscope (TEM) equipped with an INCA energy dispersive X-ray spectroscope. The lath/subgrain sizes were evaluated on TEM micrographs by the linear intercept method including all clearly visible (sub)boundaries. The dislocation density was estimated by counting the individual dislocations in the grain/subgrain interiors per unit area on at least six arbitrarily selected typical TEM images for each data point. The mean size of the secondary phase particles was evaluated on TEM micrographs. The precipitates were identified by chemical composition and diffraction pattern analysis. Other details of structural characterization and specimen preparation were reported previously [3–5, 8, 10–13]. Equilibrium fractions of phases were calculated by the Thermo-Calc software using the TCFE7 database.

3. Results

3.1. Microstructure after normalizing and tempering

Typical microstructure is presented in Fig. 1, and structural parameters are summarized in Table I.

TABLE I

Structural parameters of steel after normalization and tempering at 780 °C.

D_{PAG} [μm]	$D_{subgrains}$ [μm]	$\rho_\perp \times 10^{14}$ [m^{-2}]	d_{M23C6} [nm]	d_{VX} [nm]	d_{NbX} [nm]
20±2	0.46±0.15	2.5±1	106±3	56±5	55±5

*corresponding author; e-mail: fedoseeva@bsu.edu.ru

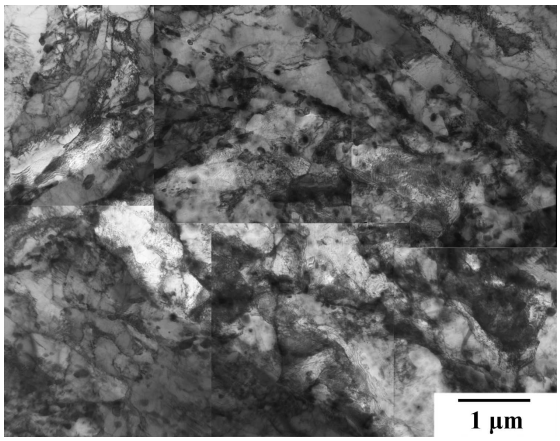

Fig. 1. TEM micrographs of the P92-type steel after normalization and tempering at 780 °C.

TABLE II

Chemical composition of secondary phase particles after tempering (wt%).

Phases	Cr	Fe	Mo	V	Nb
$M_{23}C_6$	61.26	32.97	4.37	1.41	–
V-rich MX	15.16	3.94	–	66.17	14.79
Nb-rich MX	–	2.21	–	5.08	92.71

Increasing tempering temperature from 720 [8] to 780 °C has no effect on the average size of prior austenite grains (PAGs). Part of tempered martensite lath structure (TMLS) transformed to subgrains that led to twofold decrease in lattice dislocation density [8]. The boundaries of PAGs and subgrains were decorated by nanoscale $M_{23}C_6$ carbides. No effect of tempering temperature on shape and dimensions of $M_{23}C_6$ carbides was found. In contrast, twofold increase in average of MX carbonitrides occurred with increasing tempering temperature from 720 to 780 °C [8]. Two-phase separation of MX carbonitrides on V-rich and Nb-rich particles was observed (Tables I and II). However, the mean size and shape of V- and Nb-rich MX carbonitrides were nearly the same that is not typical for tempering at ≤750 °C [1, 10]. No nanoscale V-rich MX carbonitrides with wing-like shape [1, 8] were found.

3.2. Creep properties

Creep strain vs. time and creep rate vs. time/strain curves at 650 °C and the nominal stress of 80 MPa are shown in Fig. 2. These curves are typical for 9%Cr martensitic steels containing secondary phase particles [1, 4–7].

At the applied stress of 80 MPa, the extended transient stage was observed; creep rate slowed down to the minimum value with increasing strain. Poor-defined steady-state flow could be distinguished. Minimum creep rate of $\approx 10^{-9}$ s^{-1} was approached in the strain interval 1–1.5% for ≈ 3000 h. Rupture time was 9273 h. Note that tertiary creep stage had one well-defined stage zone in contrast with 3%Co-containing P92-type steel [5, 11].

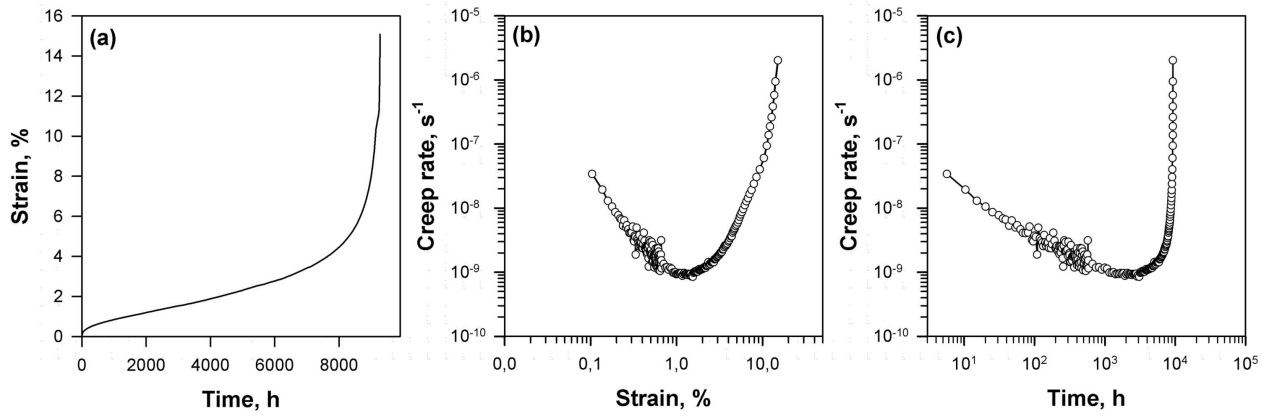

Fig. 2. Creep curves of steel studied upon creep at 650 °C, 80 MPa.

3.3. Microstructures after long-term aging and creep

Crept microstructures of the steels are shown in Fig. 3, and structural parameters are summarized in Table III.

Effect of long-term aging on microstructure and a dispersion of secondary phase particles was examined in the grip portion of samples. No effect of long-term aging on PAGs and a dispersion of MX carbonitrides was found.

In the same time, transformation of TMLS into subgrain structure occurred (Fig. 3c) that led to the insignificant decrease in lattice dislocation density. It is worth noting that no evidence for recovery and subgrain formation during long-term aging at 600 °C for ≈ 7000 h and 650 °C for ≈ 1200 h [8, 12] was found. The average size of subgrains after tempering and after long-term aging was nearly the same (Table III). The Laves phase particles precipitated at PAG and subgrain boundaries like $M_{23}C_6$ carbides under long-term aging and creep. Extensive coarsening of $M_{23}C_6$ carbides and the Laves phase up to 280 and 650 nm was found under long-term aging. Dimensions of these boundary phases were significantly higher than those after long-term aging at 650 °C for ≈ 1200 h [8].

TABLE III

Structural parameters of P92 steel after creep at 650 °C under the applied stress of 80 MPa.

Section	Reduction in area [%]	D_{PAG} [μm]	D_{subgr} [μm]	$\rho_{\perp}\times10^{14}$ [m^{-2}]	$D_{particles}$ [nm]			
					$M_{23}C_6$	Laves	VX	NbX
neck	46	20±2	1.30±0.3	0.4±0.1	300±30	650±20	90±8	60±5
gauge	8.5	20±2	0.6±0.1	1.0±0.5	290±28	550±20	80±7	60±5
grip	–	20±2	0.40±0.1	1.9±1.0	280±28	650±10	55±5	55±5

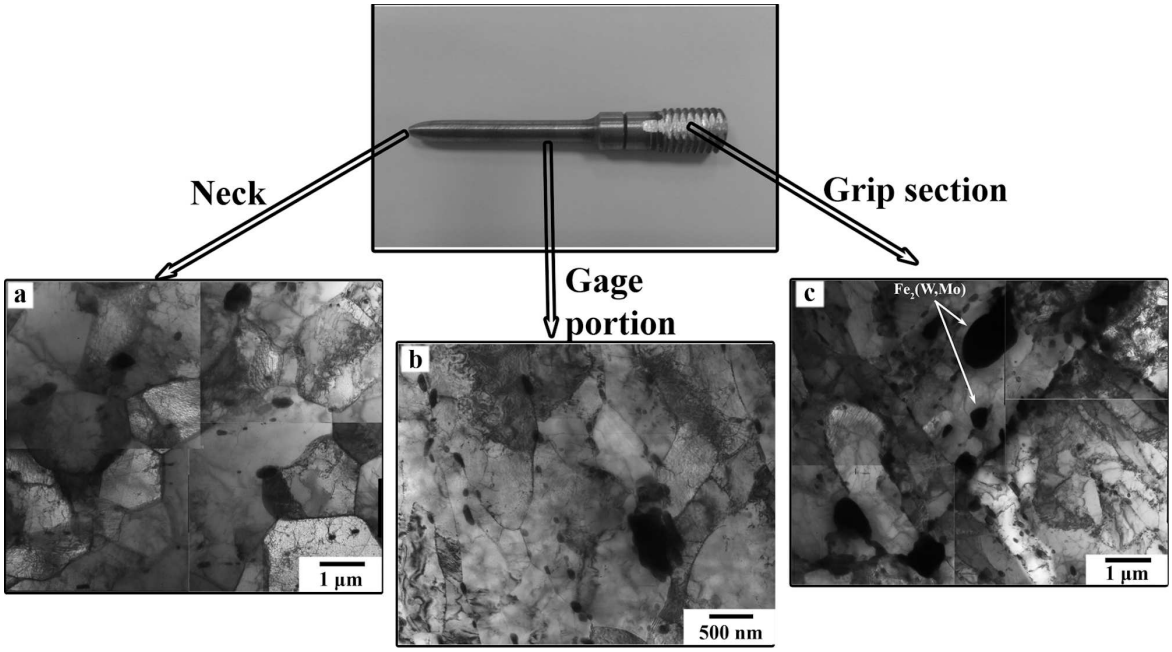

Fig. 3. Microstructures of steels studied from different sections of sample: (a) in the neck and (b) in the gauge portion (650 °C, 80 MPa), (c) in the grip section (650 °C, 9273 h).

Creep promoted subgrain growth and a decrease in dislocation density. Well-defined subgrain structure evolved in the necked portion. No strain-induced growth of $M_{23}C_6$ carbides and the Laves phase was found. $M_{23}C_6$ carbides contained ≈ 70 wt% Cr, 20–25% Fe, ≈ 5% (Mo+W) and ≈ 3% V. The Laves phase particles contained 40–45 wt% (W+Mo) and 55–60% (Fe+Cr). The W/Mo ratio in the Laves phase particles was 2–2.6. Particles of the Laves phase exhibited irregular shape and their size of ≈ 550–650 nm was nearly the same in all sections (Table III). V-rich MX particles were enriched by Nb and Cr; and Nb-rich MX particles contained traces of V, Cr and Fe after long-term aging and creep. No coarsening of Nb-rich particles with a round shape took place during long-term aging and creep, while there were few separate coarse Nb-rich particles with a size of ≈ 200 nm in all sections of specimen. Strong strain-induced coarsening of V-rich MX carbonitrides occurred in the gauge and neck sections. The size of V-rich particles increased from 55 nm to ≈ 80–90 nm after creep test (Table III).

4. Discussion

Subgrain coarsening is attributed to the balance between the pinning and the driving pressure for grain/subgrain growth. Two driving forces may induce subgrain coarsening. One of them is driving force originated from stored free lattice dislocations, and second one is driving force attributed to subboundary energy [9, 12]. No difference in dislocation density in neighbor subgrains leads to negligible driving force due to stored dislocations. Driving force originated from low-angle boundary (LAB) energy can be evaluated as [9]:

$$P_{LAB} = \frac{2\gamma}{r} = \frac{2\gamma}{\alpha D}, \tag{1}$$

where r is radius of curvature of subgrains [μm], which is proportional to grain/subgrain size D, α is constant.

The retarding force (the Zener drag) exerted by the particles, which are randomly distributed in ferritic matrix, depends on the size d [nm] and the volume fraction F_v[–] of particles as [5, 8–10, 13]:

$$P_z = 3\gamma\frac{F_v}{d}, \tag{2}$$

where γ is surface energy per unit area of the subgrain boundary [J m^{-2}]. Thus, particles exerting the retarding force must prevent the growth of subgrain structure.

An equilibrium subgrain size which may be achieved during polygonization can be estimated on the assumption of the driving and retarding forces are in a balance as follows:

$$D = \frac{2\gamma}{\alpha P_z}, \tag{3}$$

where $\alpha = 4$ [13]. The total retarding force that depends on the volume fraction and the mean size of particles affects the value of equilibrium subgrain size. The calculated values of subgrain size in the steel studied in comparison with the experimental values are presented in Table IV. It is seen that experimental subgrain size in P92-type steel is significantly lower than their equilibrium value, estimated by Eq. (3). No retarding force exerted by coarsened of $M_{23}C_6$ carbides and the Laves phase particles occurs if their sizes are more than 300 nm and 500 nm, respectively, after both long-term aging and creep. During long-term aging the subgrain growth is not controlled by coarsening of $M_{23}C_6$ carbides, the Laves phase particles and MX carbonitrides. In the grip portion, the static polygonization is not complete, because only the subgrain formation takes place, and no evidence for subgrain growth was revealed.

TABLE IV

Calculated and experimental subgrain size.

Section	D_{exper} [μm]	$D_{\text{P2=z}}$ [μm] by Eq. (3)	D_∞ [μm] by Eq. (4)	D_{modif} [μm] by Eq. (5)
neck	1.30±0.40	1.54	1.28	1.25
gauge	0.60±0.25	1.48	1.72	0.84
grip	0.40±0.10	1.27	–	–

On the other hand, the subgrain size depends on the applied stress and creep strain under creep condition and can be estimated as (4):

$$D_\infty = 10\frac{Gb}{\sigma(1+\varepsilon)}, \tag{4}$$

where G is a shear modulus [MPa], b is the Burgers vector [m], σ is an applied stress [MPa], ε is accumulated creep strain [–].

Growth of subgrain size up to the strain-induced equilibrium value by Eq. (4) indicates the completeness of recovery and polygonization processes. In the gauge section, experimental subgrain size in the P92-type steel does not reach its equilibrium value, estimated by Eq. (4), whereas in the neck, the calculated and the experimental subgrain sizes are nearly the same.

The expression (4) can be modified [14] by addition of parameters of initial structure and can be estimated as (5):

$$\log D_\infty = \log D_\infty + \log\left(\frac{D_0}{D_\infty}\right)\exp\left(-\frac{\varepsilon}{k(\sigma)}\right), \tag{5}$$

where D_0 — initial subgrain size after tempering [m], — equilibrium subgrain size from Eq. (4), ε — accumulated creep strain, $k(\sigma)$ — growth constant, 0.12 [14].

The modification of Eq. (4) by the addition of initial structure parameters gives the calculated subgrain size close to experimental one in the gauge section and the neck (Table IV). The increase in accumulated creep strain provokes the fully polygonized equiaxed structure with a very large grain size. Thus, during long-term creep the subgrain growth was determined by initial structural parameters, accumulated creep deformation and applied stress.

5. Conclusions

The microstructures of a P92-type steel tempered at 780 °C and crept at 650 °C under an applied stress of 80 MPa were studied. The main results can be summarized as follows.

1. Tempering at 780 °C led to formation of subgrain structure instead of tempered martensite lath structure (TMLS) with a mean subgrain size of 0.4 μm. $M_{23}C_6$-type particles with an average size of 105 nm precipitated on interlath and high-angle boundaries. MX carbonitrides with a mean size of 55 nm precipitated homogeneously throughout the ferritic matrix.

2. The structural changes were related to a gradual growth of ferrite subgrains and replacement of TMLS by subgrain structure. Creep strain strongly promotes this process. The mean subgrain sizes were 0.4, 0.6, and 1.3 μm in the grip section, the gauge portion and the neck, respectively.

3. During long-term creep the subgrain growth was determined by initial structural parameters, accumulated creep strain and applied stress but not by balance between driving and retarding forces.

Acknowledgments

The study was financially supported by the Russian Science Foundation, under grant No. 17-73-10380. The authors are grateful to the staff of the Joint Research Center, "Technology and Materials", Belgorod National Research University for their assistance with instrumental analysis.

References

[1] F. Abe, T.-U. Kern, R. Viswanathan, *Creep Resistant Steels*, Woodhead Publishing in Materials, Cambridge 2008, p. 678.

[2] T.-U. Kern, M. Staubli, B. Scarlin, *ISIJ Int.* **42**, 1515 (2002).

[3] R.O. Kaybyshev, V.N. Skorobogatykh, I.A. Shchenkova, *Phys. Met. Metall.* **109**, 186 (2010).

[4] A. Kipelova, M. Odnobokova, A. Belyakov, R. Kaibyshev, *Metall. Mater. Trans. A* **44A**, 577 (2013).

[5] N. Dudova, A. Plotnikova, D. Molodov, A. Belyakov, R. Kaibyshev, *Mater. Sci. Eng. A* **534**, 632 (2012).

[6] F. Abe, *Mater. Sci. Eng. A* **510-511**, 64 (2009).

[7] A. Kostka, K.-G. Tak, R.J. Hellmig, Y. Estrin, G. Eggeler, *Acta Mater.* **55**, 539 (2007).

[8] V. Dudko, A. Belyakov, D. Molodov, R. Kaibyshev, *Metall. Mater. Trans. A* **44A**, 162 (2013).

[9] F.J. Humphreys, M. Hatherly, *Recrystallization, Related Annealing Phenomena*, 2nd ed., Elsevier, Oxford 2004, p. 605.

[10] A. Fedoseeva, N. Dudova, R. Kaibyshev, *Mater. Sci. Eng. A* **654**, 1 (2016).

[11] A. Fedoseeva, N. Dudova, R. Kaibyshev, *Mater. Sci. Forum* **879**, 548 (2016).

[12] A. Fedoseeva, I. Nikitin, V. Dudko, N. Dudova, R. Kaibyshev, in: *Proc. 8th Int. Conf.: Advances in Materials Technology for Fossil Power Plants*, 2016, p. 479.

[13] A. Kipelova, R. Kaibyshev, A. Belyakov, D. Molodov, *Mater. Sci. Eng. A* **528**, 1280 (2011).

[14] W. Yan, W. Wang, Y. Shan, K. Yang, *Frontiers Mater. Sci.* **7**, 1 (2013).